European Journal of Medicinal Chemistry 95 (2015) 424–434

Contents lists available at ScienceDirect

European Journal of Medicinal Chemistry

journal homepage: http://www.elsevier.com/locate/ejmech

Original article

# Discovery of *N*-benzoxazol-5-yl-pyrazole-4-carboxamides as nanomolar SQR inhibitors

Li Xiong [a], Xiao-Lei Zhu [a, *], Yan-Qing Shen [a], Wickramabahu Kandergama Wasala Mudiyanselage Wishwajith [a], Kui Li [a], Guang-Fu Yang [a, b, *]

[a] Key Laboratory of Pesticide & Chemical Biology, College of Chemistry, Ministry of Education, Central China Normal University, Wuhan 430079, PR China
[b] Collaborative Innovation Center of Chemical Science and Engineering, Tianjing 30071, PR China

ARTICLE INFO

*Article history:*
Received 16 February 2015
Received in revised form
19 March 2015
Accepted 26 March 2015
Available online 28 March 2015

*Keywords:*
Succinate–ubiquinone oxidoreductase
Molecular design
Computational simulations
MM/PBSA
Pyrazole-carboxamides

ABSTRACT

Succinate–ubiquinone oxidoreductase (SQR, EC 1.3.5.1, complex II), an essential component of cellular respiratory chain and tricarboxylic acid (or Krebs) cycle, has been identified as one of the most significant targets for pharmaceutical and agrochemical. Herein, with the aim of discovery of new antibacterial lead structure, a series of *N*-benzoxazol-5-yl-pyrazole-4-carboxamides were designed, synthesized, and evaluated for their SQR inhibitory effects. Very promisingly, one candidate ($K_i$ = 11 nM, porcine SQR) was successfully identified as the most potent synthetic SQR inhibitor so far. The further inhibitory kinetics studies revealed that the candidate is non-competitive with respect to the substrate cytochrome *c* and DCIP. Computational simulations revealed that the titled compounds have formed hydrogen bond with D_Y91 and B_W173 and the pyrazole ring formed cation-π interaction with C_R46. In addition, in $R^1$ position, $-CHF_2$ group has increased the binding affinity and decreased the entropy contribution, while $-CF_3$ group displayed completely opposite effect when bound with SQR. The results of the present work showed that *N*-benzoxazol-5-yl-pyrazole-4-carboxamide is a new scaffold for discovery of SQR inhibitors and worth further study.



## 1. Introduction

Succinate–ubiquinone oxidoreductase (SQR, EC 1.3.5.1, complex II) is an essential component of cellular respiratory chain and tricarboxylic acid (or Krebs) cycle. The function of SQR is to catalyse the oxidation of succinate into fumarate, and coupled to the reduction of ubiquinone into ubiquinol [1–5]. Due to its critical role in the life cycle, SQR has been identified as one of the most significant targets for the development of pharmaceuticals and agrochemicals. For example, several recent studies have shown that mutant forms of SQR are responsible for causing diverse physiological disorders [6,7], leading to the hypothesis that chain B, C, and D (the crystal structure of SQR contains A, B, C, and D chains) are tumour suppressors, and that SQR is a critical component of the oxygen-sensing system [8]. A recent study reported that the 8-aminoquinoline analogue sitamaquine (SQ), an oral anti-leishmanial drug currently undergoing phase II clinical trials for the treatment of visceral leishmaniasis, caused a dose-dependent inhibition of succinate dehydrogenase of the respiratory chain in digitonin-permeabilized promastigotes, together with a drop in intracellular ATP levels and a decrease of the mitochondrial electrochemical potential [9]. In addition, in the agricultural field, over 18 SQR inhibitors have been successfully developed as agricultural fungicides, including pyrazole-4-carboxamides, oxathiin-carboxamides, phenyl-benzamides, pyridine-carboxamides, thiazole-carboxamides, phenyl-oxo-ethyl thiophene amide, pyridinyl-ethyl benzamides and furan-carboxamides [10–12]. Apart from the synthetic SQR inhibitors, Satoshi et al. reported that the natural product Atpenin A5 is a very potent SQR inhibitor, with the $IC_{50}$ 3.6 nM against bovine heart SQR and 3.7 nM against rat liver SQR [13].

Very recently, by integrating the molecular docking, molecular dynamics simulation and molecular mechanics/Poisson-Boltzmann surface area (MM/PBSA) calculations methods, we have

* Corresponding authors. College of Chemistry, Central China Normal University, Luoyu Road 152, Wuhan 430079, PR China.
*E-mail addresses:* xlzhu@mail.ccnu.edu.cn (X.-L. Zhu), gfyang@mail.ccnu.edu.cn (G.-F. Yang).

http://dx.doi.org/10.1016/j.ejmech.2015.03.060
0223-5234/

successfully established the binding mode of ten commercial carboxamide fungicides for the first time [11]. The acid moiety of carboxamide fungicides inserts into the Q-site of SQR, forming vander-Waals (VDW) interactions with C_R46, C_S42, B_I218, and B_P169, while the amine moiety extending toward the mouth of the Q-site, forming VDW interactions with C_W35, C_I43, and C_I30. The carbonyl oxygen atom of the carboxamide forms hydrogen bond with B_W173 and D_Y91. The uncovered interaction mechanism at atomic level suggested that, optimizing the important hydrogen bond interaction and improving the VDW interactions between side-chain of inhibitors and key residues in the Q-site should be an effective way to design and discover new SQR inhibitors with higher potency.

Many researches had proved that benzoxazol was an important fragment in both medicinal and agricultural chemistry. For example, fenoxaprop-P-ethyl and metamifop have been used as commercial herbicides for many years [14]. Furthermore, the benzoxazol derivatives are known to exhibit a wide range of biological activities, such as melatonin receptor agonists [15], antimicrobial [16] and anti-measles virus activities [17]. Meanwhile, pyrazole-4-carboxamides have gained a considerable attention in the field of pesticide chemistry in recent years. For example, André S et al. had reported that this type of inhibitor showed some insect activity [18]. So far, eight pyrazole-4-carboxamide derivatives have been introduced into the market as agricultural fungicides [10,19] (Fig. 1). Based on the above consideration, we proposed that pyrazole-carboxamide-benzoxazol hybrid (**7a**,**b**–**17a**,**b**) (Fig. 2) would be an new scaffold of SQR inhibitor. According the above-mentioned interaction mechanism, the benzoxadzole ring was further prolonged with substituted benzylthio group in order to increase the VDW interaction between ligand and the corresponding residues in the binding pocket. As we expected, the newly designed N-(2-(benzylthio)benzoxazol-5-yl)-pyrazole-4-carboxamides indeed showed excellent inhibitory activity against porcine SCR with the $IC_{50}$ values ranging from 0.56 to 0.038 μM, significantly higher than penthiopyrad, a commercial fungicide selected as a positive control. Among these inhibitors, compound **13b** was identified as the most promising candidate with a $K_i$ value of 11 nM against porcine SQR. The further inhibitory kinetics studies against porcine SCR (succinate–cytochrome *c* reductase) and SQR revealed that compound **13b** and penthiopyrad are both non-competitive inhibitors with respect to the substrate cytochrome *c* and dichlorophenolindophenol (DCIP). The binding mode of the titled compounds was further studied by molecular docking, molecular dynamics simulations and MM/PBSA calculations. The present work showed that *N*-benzoxazol-5-yl-pyrazole-4-carboxamide is a new scaffold for discovery of SQR inhibitors and worth further study.

## 2. Results and discussion

### 2.1. Chemistry

Title compounds **7a**,**b**–**17a**,**b** were prepared by the route shown in Scheme 1. 2-Amino-4-nitrophenol (**1**) was treated with potassium ethyl xanthate, (**2**), in ethanol to afford 5-nitrobenzo[*d*]xazol-2-thiol (**3**), which was reacted with commercially available benzyl chlorides or bromides *via* an $S_N2$ reaction to obtain the key intermediates **4a**–**k** in good yields. The nitrobenzoxazols **4a**–**k** were refluxed in ethanol/$H_2O$ with powered iron in the presence of $NH_4Cl$ to provide amines **5a**–**k**, which were used without purification. Finally, compounds **5a**–**k** were then subjected to an amide formation reaction with pyrazole carboxylic acids **6** by using EDCI as the coupling reagent to furnish the final products **7**–**17a**/**b** in 45–80% yield. Structures of all the target compounds were characterized by $^1H$ NMR, $^{13}C$ NMR and HRMS spectral data.

### 2.2. Enzyme inhibition

Succinate–cytochrome *c* reductase (SCR) is the mixture of respiratory complex II and complex III, which was also deemed to form complex II–complex III super complexes. Complex II (SQR) firstly passes electrons from succinate to ubiquinone, and then complex III passes electrons from reduced ubiquinone to cytochrome *c*. The activity of SQR in SCR was selectively determined by using succinate and dichlorophenolindophenol (DCIP) as substrates, and the activity of only complex III in SCR was determined by using decylubiquinol ($DBH_2$) and cytochrome *c* as substrates, whereas the overall activity of SCR (both complex II and complex III) was determined using succinate and cytochrome *c* as substrates [11].

The enzymatic inhibition of all newly synthesized compounds **7**–**17** against porcine SCR was assayed and the determined $IC_{50}$ values against porcine SCR were listed in Table 1. For comparison, the inhibitory activity of the corresponding pyrazole-4-carboxamide commercial fungicide penthiopyrad was also presented. The results indicated that all of the compounds exhibited no effect on the activity of complex III (data not show), but markedly inhibited the activity of SCR. As shown in Table 1, 22 new synthesized compounds showed a significant improvement of SCR inhibitory activity than penthiopyrad, which indicated that the introduction of benzoxazol with substituted benzylthio group was reasonable. Remarkably, the analogues **7a**–**17a** bearing the $R^1$ group of $-CF_3$ always displayed lower activity than **7b**–**17b** with $-CHF_2$. For instance, the $IC_{50}$ value against SCR of **13b** ($R^1 = -CHF_2$) was 0.038 μM, while that of **13a** ($R^1 = -CF_3$) was 0.088 μM. In addition, other compounds had also displayed the same phenomenon, suggesting that the $-CHF_2$ group is critical to maintain high potency and its molecular mechanism would be discussed in the

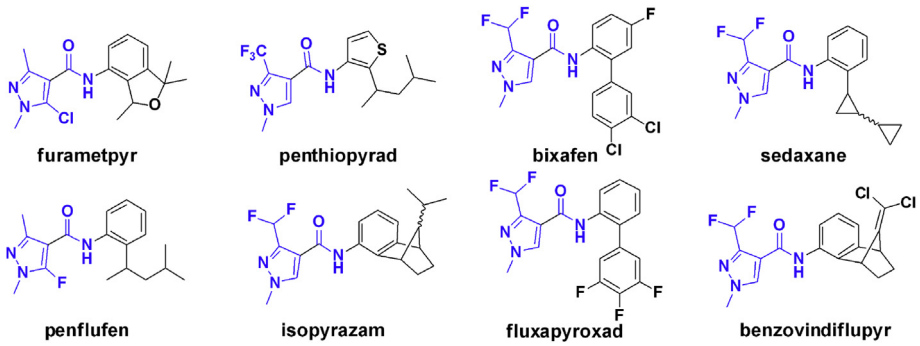


**Fig. 1.** Structures of pyrazole-4-carboxamides SQR inhibitors.

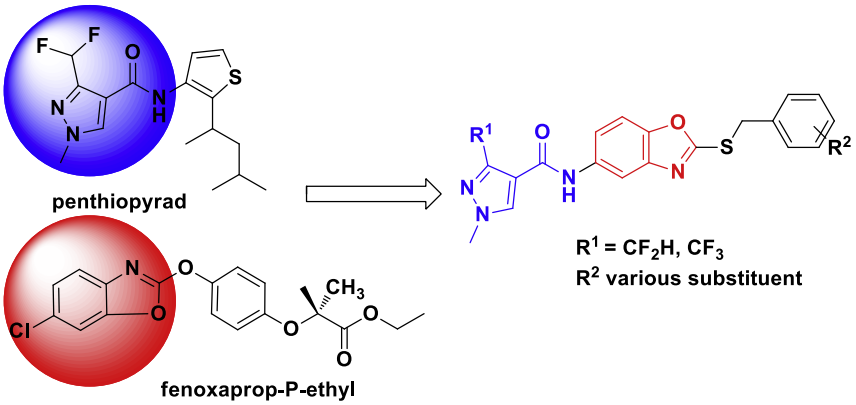


**Fig. 2.** Design strategy of the title compounds.

following section. Obviously, the inhibitory activities were varied with regard to the different groups at the 3-position and/or 4-position of phenyl. It seemed that introducing electron-withdrawing group at phenyl 4-position produced a higher SCR inhibition effect than 3-position. Taking the chlorine substituent as an example, compounds **9a** (4-Cl, $IC_{50}$ = 0.111 μM) and **9b** (4-Cl, $IC_{50}$ = 0.057 μM) showed higher activity than compounds **15a** (3-Cl, $IC_{50}$ = 0.149 μM) and **15b** (3-Cl, $IC_{50}$ = 0.082 μM). Compounds **8a** (4-F, $IC_{50}$ = 0.210 μM) and **8b** (4-F, $IC_{50}$ = 0.101 μM) also showed higher activity than **11a** (3-F, $IC_{50}$ = 0.418 μM) and **11b** (3-F, $IC_{50}$ = 0.244 μM). In addition, the electron-withdrawing $R^2$ groups had a favourable effect on the inhibitory activity than electron-donating group, except −CN. For example, compound **7** (4-$CF_3$) and **8** (4-F) showed higher activity than **14** (4-OMe) and **16** (4-Me), respectively. Compared with the single fluorine substituted derivatives (*e.g.* compounds **8** and **11**), compounds **17** with 3,4-di-F at $R^2$ position displayed increased inhibitory activity upon porcine SCR, indicating that the disubstituted group at the phenyl might be more favourable for the activity than mono substituted group. One possibility for this phenomenon is that $R^1$ and $R^2$ would affect the bioactive conformation of inhibitors.

Kinetic properties are of great importance for understanding the molecular mechanism of SQR function. We therefore selected **13b** as an example to study the mechanism of SCR and SQR inhibition. As shown in Fig. 3A, double-reciprocal plots showed non-competitive inhibition of **13b** with respect to cytochrome *c*. Furthermore, we examined the effect of **13b** on the reactions of the SCR pathway catalysed by SQR. We determined the kinetics of SQR activity with respect to the substrate DCIP in the absence and presence of **13b**. As shown in Fig. 3B, **13b** was a non-competitive inhibitor against SQR with respect to the substrate DCIP. These results indicate that **13b** would bind to the Q-site of SQR, consistent with our previous study [11] that the carboxamide inhibitors bind to the Q-site of SQR. A similar result was obtained for commercial fungicide penthiopyrad. As shown in Fig. 3C and D, penthiopyrad is a non-competitive inhibitor with respect to cytochrome *c* ($K_i$ = 1.393 μM) and DCIP ($K_i$ = 0.327 μM).

Next, we compared the inhibitory activities of both of compound against porcine SCR and SQR (Table 2 and Fig. 3). Compound **13b** and penthiopyrad exhibited about 4-fold greater inhibition against the porcine SQR than SCR, as indicated by the $K_i$ values. We also found that compound **13b** and penthiopyrad nearly did not show inhibitory effects against complex III at 10 μM concentrations (the inhibition rate was about 13% for **13b** and lower than 10% for penthiopyrad). Furthermore, we also measured the $IC_{50}$ values of **13b** and penthiopyrad against porcine SQR (Supporting information Fig. 1S). The difference in $IC_{50}$ values was still very small. All these results indicated that the portion of complex III in SCR system did not display effect upon the SQR assay. In addition, **13b** should have the same mechanism of biological action with commercial fungicide. As shown in Table 2, the $K_i$ value of **13b** was 0.043 μM against porcine SCR and 0.011 μM against porcine SQR, which was about 30-fold higher activity than penthiopyrad. Therefore, to our knowledge, compound **13b** is so far the most potent synthetic inhibitor of SQR.

### 2.3. The binding free energy calculation

To understand the structure–activity relationship at the atomic level, we performed the molecular docking and binding free energy

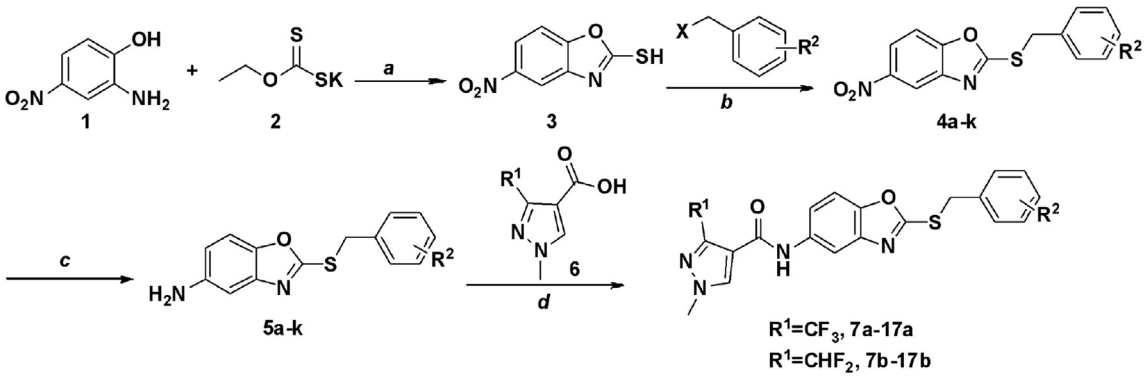


**Scheme 1.** Synthesis of compounds **7**–**17a**/**b**. Reagents and conditions: (*a*) EtOH, reflux; (*b*) substituted benzyl chloride/bromide, $K_2CO_3$, acetone, reflux; (*c*) EtOH/$H_2O$, $NH_4Cl$, reflux, addition of Fe; (*d*) carboxylic acid **6**, EDCI, DMAP, $CH_2Cl_2$, r. t.

**Table 1**
Inhibitory activities and the binding free energy of compounds **7**–**17** against porcine SCR.

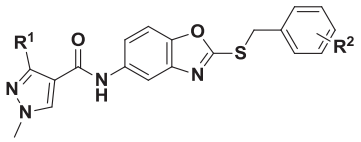

| No. | $R^1$ | $R^2$ | $\Delta E_{ele}$ | $\Delta E_{vdw}$ | $\Delta G_{np}$ | $\triangle G_{pol}$ | $\Delta H$ | $-T\Delta S$ | $\Delta G_{cal}$ | $\Delta G_{exp}$[a] | $IC_{50}$ (μM) |
|---|---|---|---|---|---|---|---|---|---|---|---|
| **7a** | $CF_3$ | 4-$CF_3$ | −19.32 | −45.72 | −5.37 | 43.96 | −26.44 | 10.61 | −15.83 | −9.62 | 0.083 ± 0.001 |
| **7b** | $CHF_2$ | 4-CF3 | −24.21 | −44.94 | −5.31 | 46.54 | −27.91 | 11.47 | −16.44 | −10.07 | 0.039 ± 0.001 |
| **8a** | $CF_3$ | 4-F | −19.98 | −44.19 | −5.22 | 44.53 | −24.86 | 10.20 | −14.66 | −9.07 | 0.210 ± 0.019 |
| **8b** | $CHF_2$ | 4-F | −23.36 | −43.23 | −5.15 | 45.41 | −26.33 | 10.94 | −15.39 | −9.51 | 0.101 ± 0.012 |
| **9a** | $CF_3$ | 4-Cl | −18.59 | −44.53 | −5.24 | 42.92 | −25.44 | 10.43 | −15.01 | −9.45 | 0.111 ± 0.001 |
| **9b** | $CHF_2$ | 4-Cl | −22.67 | −44.19 | −5.20 | 44.83 | −27.23 | 11.10 | −16.13 | −9.84 | 0.057 ± 0.001 |
| **10a** | $CF_3$ | 4-CN | −22.99 | −44.64 | −5.40 | 48.90 | −24.13 | 11.23 | −12.90 | −8.49 | 0.562 ± 0.011 |
| **10b** | $CHF_2$ | 4-CN | −21.97 | −43.56 | −5.04 | 44.56 | −26.01 | 12.39 | −13.62 | −8.70 | 0.397 ± 0.012 |
| **11a** | $CF_3$ | 3-F | −18.20 | −43.83 | −5.21 | 42.45 | −24.80 | 10.82 | −13.98 | −8.67 | 0.418 ± 0.011 |
| **11b** | $CHF_2$ | 3-F | −21.93 | −43.48 | −5.14 | 44.51 | −26.03 | 11.79 | −14.24 | −8.99 | 0.244 ± 0.012 |
| **12a** | $CF_3$ | 3-Br | −22.49 | −43.97 | −5.19 | 45.53 | −26.12 | 10.54 | −15.58 | −9.41 | 0.119 ± 0.001 |
| **12b** | $CHF_2$ | 3-Br | −24.07 | −45.98 | −5.24 | 48.13 | −27.17 | 11.14 | −16.03 | −9.79 | 0.062 ± 0.001 |
| **13a** | $CF_3$ | 4-$OCF_3$ | −17.84 | −47.78 | −5.44 | 45.76 | −25.29 | 9.70 | −15.59 | −9.59 | 0.088 ± 0.010 |
| **13b** | $CHF_2$ | 4-$OCF_3$ | −26.86 | −43.74 | −5.34 | 47.52 | −28.41 | 11.46 | −16.95 | −10.08 | 0.038 ± 0.001 |
| **14a** | $CF_3$ | 4-OMe | −20.67 | −45.38 | −5.40 | 45.73 | −25.73 | 11.50 | −14.23 | −8.90 | 0.284 ± 0.012 |
| **14b** | $CHF_2$ | 4-OMe | −23.03 | −45.88 | −5.35 | 46.31 | −27.95 | 13.82 | −14.13 | −9.08 | 0.208 ± 0.013 |
| **15a** | $CF_3$ | 3-Cl | −15.11 | −43.49 | −5.19 | 42.37 | −21.41 | 7.00 | −14.41 | −9.28 | 0.149 ± 0.015 |
| **15b** | $CHF_2$ | 3-Cl | −23.16 | −45.78 | −5.20 | 47.73 | −26.41 | 10.70 | −15.71 | −9.63 | 0.082 ± 0.001 |
| **16a** | $CF_3$ | 4-Me | −23.31 | −43.28 | −5.22 | 47.93 | −23.88 | 10.04 | −13.84 | −8.93 | 0.269 ± 0.012 |
| **16b** | $CHF_2$ | 4-Me | −25.68 | −44.44 | −5.21 | 48.49 | −26.85 | 12.26 | −14.59 | −9.05 | 0.216 ± 0.010 |
| **17a** | $CF_3$ | 3,4-di-F | −14.77 | −45.63 | −5.25 | 42.01 | −23.65 | 8.50 | −15.15 | −9.36 | 0.130 ± 0.012 |
| **17b** | $CHF_2$ | 3,4-di-F | −22.21 | −41.35 | −4.86 | 42.92 | −25.49 | 10.17 | −15.32 | −9.51 | 0.100 ± 0.001 |
| Penthiopyrad | | | −13.84 | −41.91 | −5.10 | 34.28 | −26.57 | 13.54 | −13.03 | −7.99 | 1.321 ± 0.11 |

[a] $\Delta G_{exp} = -RTLnIC_{50}$.

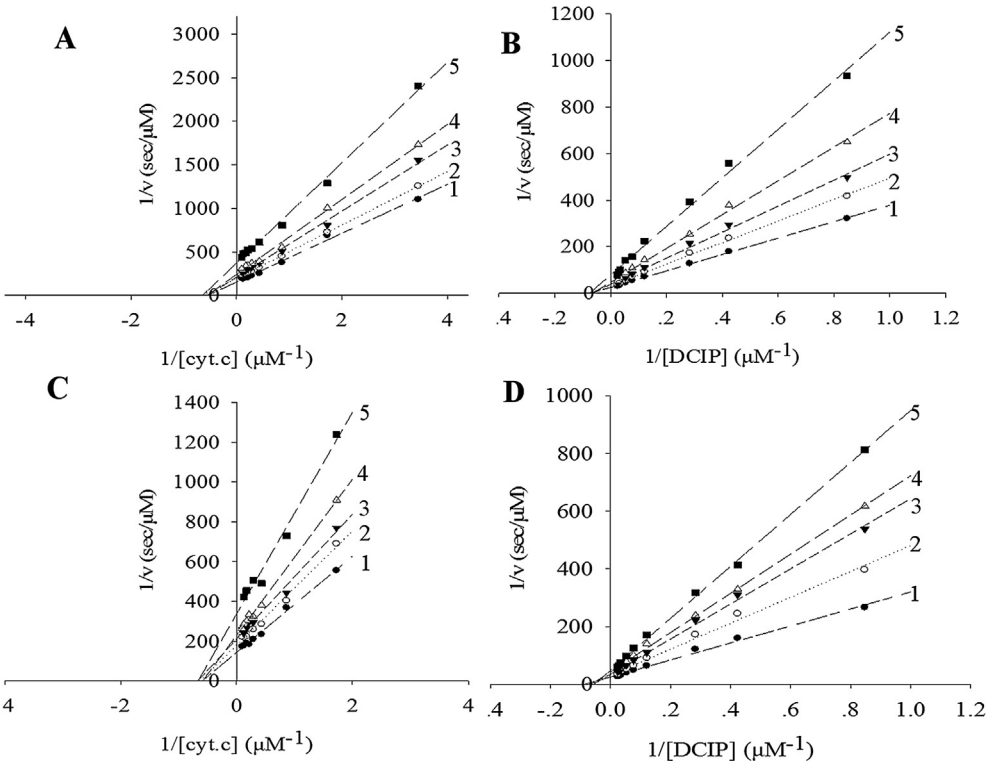


**Fig. 3.** Kinetic analysis of inhibition by **13b** (A for SCR and B for SQR) and penthiopyrad (C for SCR and D for SQR) against porcine SCR and SQR. The inhibition of porcine SCR by (A) **13b** (1, 0 nM; 2, 10 nM; 3, 20 nM; 4, 30 nM and 5, 50 nM), (C) penthiopyrad (1, 0 nM; 2, 300 nM; 3, 500 nM; 4, 1000 nM and 5, 2000 nM). Each reaction mixture contains 100 mM PBS (pH 7.4), 0.3 mM EDTA, 20 mM succinate, 0.1 nM enzyme, 0.29–10.36 μM cytochrome *c* and the indicated penthiopyrad or **13b**. $K_i$ was estimated to be 0.043 ± 0.002 μM for **13b** and 1.393 ± 0.087 μM for penthiopyrad by assuming non-competitive inhibition. The inhibition of porcine SQR by (B)**13b** (1, 0 nM; 2, 3 nM; 3, 5 nM; 4, 10 nM and 5, 20 nM), (D) penthiopyrad (1, 0 nM; 2, 100 nM; 3, 200 nM; 4, 300 nM and 5, 500 nM). Each reaction mixture contains 100 mM PBS (pH 7.4), 0.3 mM EDTA, 20 mM succinate, 2 nM SCR, 1.18–41.22 μM DCIP and the indicated amount of penthiopyrad or **13b**. $K_i$ was estimated to be 0.011 ± 0.0003 μM for **13b** and 0.327 ± 0.0092 μM for penthiopyrad by assuming non-competitive inhibition.

**Table 2**
The inhibitory effect of some inhibitors against porcine SCR and SQR.

| Inhibitor | SCR (succinate-cyt. *c* system 23 °C) | | | SQR (DCIP-system 23 °C) | | |
|---|---|---|---|---|---|---|
| | $IC_{50}$ (μM) | Inhibition type (with cyt. *c*) | $K_i$ (μM) | $IC_{50}$ (μM) | Inhibition type (with DCIP) | $K_i$ (μM) |
| **13b** | 0.038 ± 0.001 | Non-competitive | 0.043 ± 0.002 | 0.011 ± 0.0011 | Non-competitive | 0.011 ± 0.0003 |
| Penthiopyrad | 1.321 ± 0.110 | Non-competitive | 1.3931 ± 0.087 | 0.527 ± 0.111 | Non-competitive | 0.327 ± 0.0092 |

calculations for all newly synthesized compounds. As summarized in Table 1, the calculated binding free energies ($\Delta G_{cal}$) range from −12.90 kcal/mol to −16.95 kcal/mol, whereas the experimental binding free energies ($\Delta G_{exp}$) range from −8.49 kcal/mol to −10.08 kcal/mol. Obviously, the MM/PBSA calculations systematically overestimated the absolute binding affinities of the ligand toward SQR. However, the relative order of the calculated binding affinities of the compounds is qualitatively consistent with the order of potency. A good linear correlation between $\Delta G_{cal}$ and $\Delta G_{exp}$ was obtained with a correlation coefficient of $R^2 = 0.93$ (Fig. 4), confirming the reliability of the computational models constructed in this study. At the same time, the correlation coefficients between $\Delta G_{exp}$ and individual energy terms are 0.16 for sum of the electrostatic energies ($\Delta E_{ele}$), 0.12 for sum of the VDW energies ($\Delta E_{vdw}$), 0.03 for nonpolar solvation energies ($\Delta G_{np}$), 0.18 for polar solvation energies ($\Delta G_{pol}$), 0.13 for enthalpy contribution ($\Delta H$), and 0.10 for entropy compensation ($-T\Delta S$). The results of the individual energy terms suggest that, although the enthalpy contribution ($\Delta H$) is important for binding, the binding free energy arises from a more complex interplay among these components. Indeed, the ELE (ranging from −14.77 to −26.86 kcal/mol) and VDW (ranging from −41.35 to −47.78 kcal/mol) energies are the larger favourable components of the binding free energy for each complex. This result indicates that the affinities of these inhibitors for SQR are dominated by electronic interaction and shape complementarily.

As shown in Table 1, compound **13b** was the most potent inhibitor with the $K_i$ value of 0.011 μM against porcine SQR. The simulated binding mode **13b** (Fig. 5A) showed that the carbonyl oxygen atom formed hydrogen bond with the residue of D_Y91 and B_W173 and pyrazole ring formed cation-π interaction with the residue of C_R46, which were nearly the same as the commercial carboxamide fungicides obtained in our previous work [11]. In addition, the hydrogen atom in $-CHF_2$ group also formed hydrogen bond with the residue of D_D90 and the phenyl ring formed hydrophobic interaction with D_Y91. Other compounds also displayed the similar binding mode. As shown in Table 1, the compounds **7b**–**17b** always showed higher activities against SCR than **7a**–**17a**.

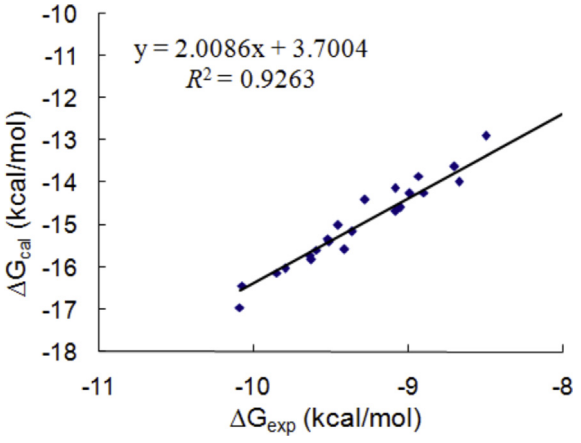


**Fig. 4.** Correlation between the calculated and experimental binding free energy.

In order to illustrate the phenomena, the binding modes of **7b**–**17b** were superimposed and we found that there were about two space conformations for the hydrogen atom in $-CHF_2$ group in $R^1$ position. One was the same as **13b**, in which the hydrogen atom in $-CHF_2$ group formed hydrogen bond with D_D90. The other was that the hydrogen atom in $-CHF_2$ group pointed to carbonyl oxygen atom and then formed intramolecular hydrogen bond with it (Fig. 5B). One possible reason for this phenomenon might be due to the group effect in $R^2$ position. The $-CHF_2$ in **7b**, **8b**, **10b**, **12b**, **13b**, **15b**, **16b** and **17b** (Fig. 5B) displayed the same conformation with **13b**, and others (including **9b**, **11b**, and **14b**, Fig. 5C) took on another conformation. Therefore, when replacing the $-CHF_2$ group at $R^1$ position with $-CF_3$, **7a**–**17a** compounds would lose hydrogen bond with D_D90 or intramolecular hydrogen bond with carbonyl oxygen atom, which contributed greatly to the potency of SQR inhibitors (Fig. 5D).

Based on above analysis, it seemed that $-CF_3$ group in $R^1$ position would lead to unfavourable interaction when bound with SQR. From the energy component analysis (Table 1), we concluded that the compounds **7b**–**17b** always showed more favourable electronic energy ($\Delta E_{ele}$) and binding affinity ($\Delta H$) bound with SQR than **7a**–**17a**. On the contrary, the entropy compensation ($-T\Delta S$) in **7b**–**17b** was less favourable than **7a**–**17a**. All these results indicated that, in $R^1$ position, $-CHF_2$ group would increase the binding affinity and decrease the entropy contribution when bound with SQR, while $-CF_3$ group displayed completely opposite effect.

At the same time, we also found that the substituted phenyl ring showed different conformations when bound with SQR. This might be due to rotatable single bonds between benzoxazol and phenyl ring. For example (Fig. 5C), 4-Cl substituted phenyl in **9b** would form edge-to-edge π–π interaction with C_W35, and 3-F substituted phenyl in **11b** would point to another direction forming hydrophobic interaction with C_I30 and C_T31 (data not show).

When the $R^2$ group changed from 4-$OCF_3$ to 4-CN, 4-OMe, 4-Me or 3-F, compounds would show less activity, such as **10a** and **10b**, **14a** and **14b**, **16a** and **16b**. In order to understand the molecular basis of this phenomenon, the interaction energy between inhibitor and key residues was calculated *via* Anal module. For instance, the interaction energy, including electronic and VDW energy, between ligands with B_W173 and D_Y91 respective are −9.83 and −8.98 kcal/mol for **10a** ($R^2$ = 4-CN), −10.50 and −9.30 kcal/mol for **10b** ($R^2$ = 4-CN), −11.99 and −9.60 kcal/mol for **14a** ($R^2$ = 4-OMe), −8.38 and −5.79 kcal/mol for **14b** ($R^2$ = 4-OMe), −12.30 and −10.95 kcal/mol for **16a** ($R^2$ = 4-Me), −15.09 and −12.08 kcal/mol for **16b** ($R^2$ = 4-Me), −14.71 and −12.03 kcal/mol for **13b** ($R^2$ = 4-$OCF_3$), respectively. Hence, excepting **16b**, the replacement of 4-$OCF_3$ with 4-CN, 4-OMe, 4-Me or 3-F may result in the lower interaction energy with key residues and then less binding free energy with SQR. As for **16b**, less favourable entropy contribution ($-T\Delta S$) might be used to explain its lower activity.

## 3. Conclusions

In summary, a series of novel *N*-(2-(benzylthio)benzoxazol-5-yl)-pyrazole-4-carboxamide **7**–**17** were designed and synthesized as potent SQR inhibitors, among which 3-(difluoromethyl)-1-

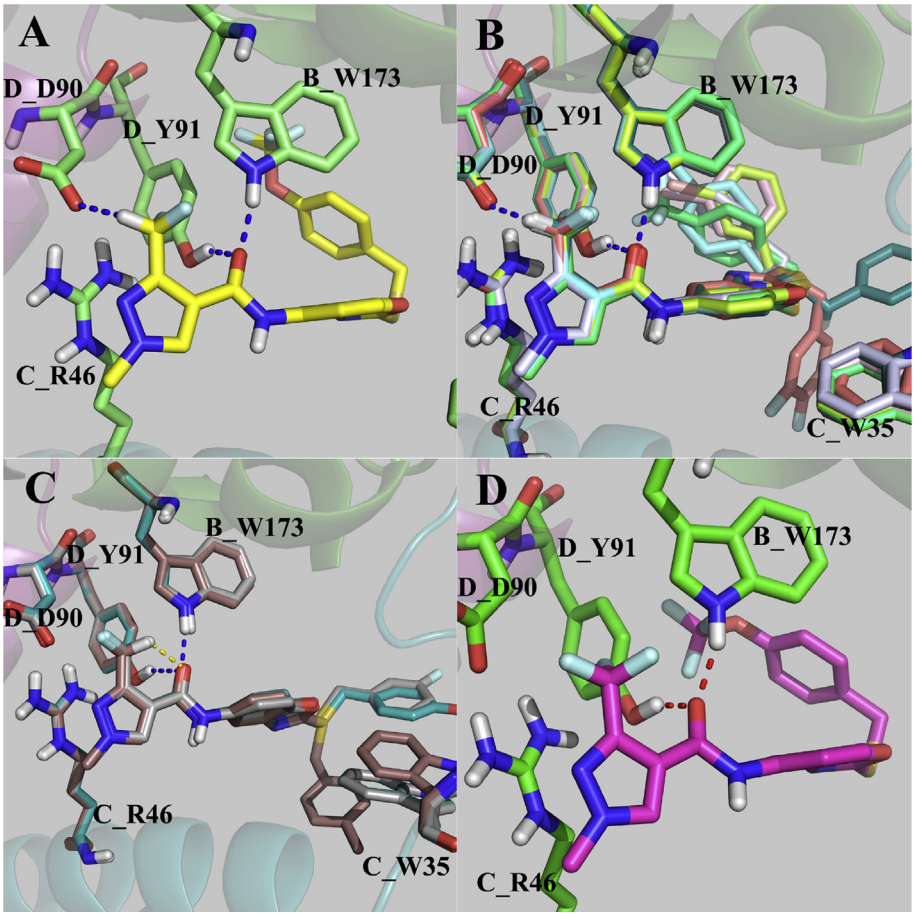


**Fig. 5.** (A) The binding mode of **13b**. The blue dashed line represent the hydrogen bond between **13b** and key residues; (B) The binding mode overlay of **7b** (ice green), **8b** (dark blue), **10b** (grey), **12b** (yellow), **15b** (pink), **16b** (ice blue), and **17b** (dark red). For clarity, only hydrogen bond between **7b** and key residues was shown as blue dashed line; (C) The binding mode overlay of **9b** (brown), **11b** (grey), and **14b** (blue). For clarity, only hydrogen bond between **9b** and key residues was shown as blue dash line and the intramolecule hydrogen bond was coloured by yellow; (D) The binding mode of **13a**. (For interpretation of the references to colour in this figure legend, the reader is referred to the web version of this article.)

methyl-*N*-(2-((4-(trifluoromethoxy)benzyl)thio)-benzoxazol-5-yl)-*1H*-pyrazole-4-carboxamide **13b** was identified as the most potent candidate with $K_i$ value of 11 nM against porcine SQR. The further inhibitory kinetics studies showed that **13b** is a non-competitive inhibitor with respect to substrate cytochrome *c* and DCIP. In addition, the results of computational simulations revealed that the title compound binds with the Q-site of SQR, forming hydrogen-bonds with D_Y91 and B_W173 and cation-$\pi$ interaction between its pyrazole ring and C_R46. Meanwhile, the $-CHF_2$ group at $R^1$ position formed additional hydrogen bond with D_D90 and/or intramolecular hydrogen bond with carbonyl oxygen, contributing significantly to the potency of SQR inhibitors. According to the results of energy component analysis, we concluded that the $-CHF_2$ group at $R^1$ position would increase the binding affinity and decrease the entropy contribution, while $-CF_3$ group at this position took on opposite effect. Therefore, how to balance the binding affinity and entropy contribution would be the primary concern in our future work.

## 4. Materials and methods

### 4.1. Reagents and equipment

Unless otherwise noted, all chemical and biological reagents were commercially available and treated with standard methods before use. Solvents were dried in a routine way and redistilled before use. $^1H$ NMR and $^{13}C$ NMR spectra were recorded on a VARIAN Mercury-Plus 600 or a 400 spectrometer in $CDCl_3$ or DMSO-$d_6$ with TMS as internal reference. Mass spectral data were obtained on a Thermo Fisher Mass platform DSQII by electrospray ionization (ESI-MS). High resolution mass spectra (HRMS) were acquired in positive mode on a WATERS MALDI SYNAPT G2 HDMS (MA, USA). Melting points were taken on a Büchi B-545 melting point apparatus and were uncorrected. All chemical yields were not optimized and generally represent the result of a single experiment.

### 4.2. Synthesis of the intermediate **3** [20]

A solution of 2-amino-4-nitrophenol (7.7 g, 50 mmol) in ethanol (100 mL) was heated to reflux, and potassium ethyl xanthate (8.4 g, 55 mmol) was added at reflux temperature. The resulting mixture was refluxed for 4 h and then it was allowed to cool to ambient temperature, then the solution was poured into water and aqueous hydrochloric acid was added. The resulting precipitate was collected by filtration, washed with water and dried to afford 16.5 g (84%) 5-nitrobenzoxazol-2-thiol.

### 4.3. General procedure for synthesis of the intermediate **4a–k** [21]

Potassium carbonate (6.0 mmol) and the corresponding halide derivative (5.5 mmol) were added to 5 mmol of stirred solution of intermediate **3** in acetone (50 mL). When the reaction was completed, as monitored by TLC detection, the reaction mixture was filtered and the solvent was removed under reduced pressure. The residue was purified by column chromatography on silica gel.

#### 4.3.1. Data for **4a**

Yellow solid; yield: 78%; mp 130–132 °C; $^1$H NMR (600 MHz, $CDCl_3$) $\delta$ 8.50 (s, 1H), 8.24 (d, $J$ = 9.0 Hz, 1H), 7.62–7.60 (m, 4H), 7.54 (d, $J$ = 9.0 Hz, 1H), 4.61 (s, 2H); MS (EI) $m/z$: 354.12 $(M)^+$.

#### 4.3.2. Data for **4b**

White solid; yield: 72%; mp 133–135 °C; $^1$H NMR (600 MHz, $CDCl_3$) $\delta$ 8.50 (d, $J$ = 2.4 Hz, 1H), 8.24 (dd, $J$ = 9.0, 2.4 Hz, 1H), 7.54 (d, $J$ = 9.0 Hz, 1H), 7.47(dd, $J$ = 8.4, 4.2 Hz, 2H), 7.06 (t, $J$ = 9.0 Hz, 2H), 4.56 (s, 2H); MS (EI) $m/z$: 304.25 $(M)^+$.

#### 4.3.3. Data for **4c**

White solid; yield: 73%; mp 132–133 °C; $^1$H NMR (600 MHz, $CDCl_3$) $\delta$ 8.50 (d, $J$ = 1.8 Hz, 1H), 8.24 (dd, $J$ = 8.4, 1.8 Hz, 1H), 7.54 (d, $J$ = 9.0 Hz, 1H), 7.43 (d, $J$ = 9.6 Hz, 2H), 7.33 (s, 2H), 4.54 (s, 2H); MS (EI) $m/z$: 320.15 $(M)^+$.

#### 4.3.4. Data for **4d**

White solid; yield: 75%; mp 160–162 °C; $^1$H NMR (600 MHz, $CDCl_3$) $\delta$ 8.50 (d, $J$ = 1.8 Hz, 1H), 8.25 (dd, $J$ = 9.0, 2.4 Hz, 1H), 7.66 (d, $J$ = 7.8 Hz, 2H), 7.63 (d, $J$ = 8.4 Hz, 2H), 7.54 (d, $J$ = 9.0 Hz, 1H), 4.59 (s, 2H); MS (EI) $m/z$: 311.16 $(M)^+$.

#### 4.3.5. Data for **4e**

White solid; yield: 79%; mp 101–103 °C; $^1$H NMR (600 MHz, $CDCl_3$) $\delta$ 8.50 (d, $J$ = 1.8 Hz, 1H), 8.24 (dd, $J$ = 9.0, 2.4 Hz, 1H), 7.54 (d, $J$ = 9.0 Hz, 1H), 7.33 (d, $J$ = 5.4 Hz, 1H), 7.25 (s, 1H), 7.21 (d, $J$ = 9.6 Hz, 1H), 7.02(t, $J$ = 8.4 Hz, 1H), 4.56 (s, 2H); MS (EI) $m/z$: 304.17 $(M)^+$.

#### 4.3.6. Data for **4f**

White solid; yield: 85%; mp 104–105 °C; $^1$H NMR (600 MHz, $CDCl_3$) $\delta$ 8.50 (d, $J$ = 1.8 Hz, 1H), 8.25(dd, $J$ = 9.0, 2.4 Hz, 1H), 7.65 (s, 1H), 7.45 (dd, $J$ = 8.4, 2.4 Hz, 2H), 7.26 (s, 1H), 7.24 (d, $J$ = 7.8 Hz, 1H), 4.53 (s, 2H); MS (EI) $m/z$: 364.15 $(M)^+$.

#### 4.3.7. Data for **4g**

White solid; yield: 68%; mp 126–128 °C; $^1$H NMR (600 MHz, $CDCl_3$) $\delta$ 8.52 (d, $J$ = 2.4 Hz, 1H), 8.24 (dd, $J$ = 9.0, 2.4 Hz, 1H), 7.44 (d, $J$ = 9.0 Hz, 1H), 6.98 (d, $J$ = 8.4 Hz, 2H), 6.88 (d, $J$ = 9.0 Hz, 2H), 4.56 (s, 2H); MS (EI) $m/z$: 370.22 $(M)^+$.

#### 4.3.8. Data for **4h**

White solid; yield: 76%; mp 135–137 °C; $^1$H NMR (600 MHz, $CDCl_3$) $\delta$ 8.49 (s, 1H), 8.23 (d, $J$ = 8.4 Hz, 1H), 7.53(dd, $J$ = 8.4, 2.4 Hz, 1H), 7.40 (d, $J$ = 7.8 Hz, 2H), 6.89 (d, $J$ = 7.8 Hz, 2H), 4.55 (s, 2H), 3.80 (s, 3H); MS(EI) $m/z$: 316.18 (M)+.

#### 4.3.9. Data for **4i**

White solid; yield: 82%; mp 100–102 °C; $^1$H NMR (600 MHz, $CDCl_3$) $\delta$ 8.49 (d, $J$ = 1.8 Hz, 1H), 8.23 (dd, $J$ = 8.4, 1.8 Hz, 1H), 7.53 (d, $J$ = 9.0 Hz, 1H), 7.37 (d, $J$ = 7.8 Hz, 2H), 7.17 (d, $J$ = 7.2 Hz, 2H), 4.53 (s, 2H); MS (EI) $m/z$: 320.16 $(M)^+$.

#### 4.3.10. Data for **4j**

White solid; yield: 84%; mp112-114 °C; $^1$H NMR (600 MHz, $CDCl_3$) $\delta$ 8.50 (d, $J$ = 1.8 Hz, 1H), 8.24 (dd, $J$ = 8.4, 1.8 Hz, 1H), 7.53 (d, $J$ = 8.4 Hz, 1H), 7.37 (d, $J$ = 7.8 Hz, 2H), 7.17 (d, $J$ = 7.2 Hz, 2H), 4.56 (s, 2H), 2.35 (s, 3H); MS (EI) $m/z$: 300.33 $(M)^+$.

#### 4.3.11. Data for **4k**

White solid; yield: 70%; mp 101–102 °C; $^1$H NMR (600 MHz, $CDCl_3$) $\delta$ 8.50 (s, 1H), 8.25 (dd, $J$ = 7.2, 1.8 Hz, 1H), 7.54 (d, $J$ = 9.0 Hz, 1H), 7.35–7.33 (m, 1H), 7.23 (dd, $J$ = 6.6, 1.8 Hz, 1H), 7.16 (dd, $J$ = 18.0, 8.4 Hz, 1H), 4.52 (s, 2H); MS(EI) $m/z$: 322.16 $(M)^+$.

### 4.4. Synthesis of the intermediate **5a–k** [22]

The intermediate **4** (3.2 mmol) and ammonium chloride (0.171 g, 3.2 mmol) were dissolved in a mixture of ethanol (50 mL) and water (6 mL). The reaction mixture was heated to reflux and powered iron (0.536 g, 9.6 mmol) was added at reflux temperature. After completing the reaction, the resulting mixture was filtered through diatomaceous earth and the filtrate was concentrated under reduced pressure. The residue was extracted with ethyl acetate, and the combined extracts were washed with saturated brine. Finally, the residue was purified by column chromatography on silica gel.

#### 4.4.1. Data for **5a**

White solid; yield: 81%; mp 99–101 °C; $^1$H NMR (600 MHz, $CDCl_3$) $\delta$ 7.58–7.56 (m, 4H), 7.21 (d, $J$ = 8.4 Hz, 1H), 6.90 (s, 1H), 6.60 (d, $J$ = 7.8 Hz, 1H), 4.54 (s, 2H); MS (EI) $m/z$: 324.15 $(M)^+$.

#### 4.4.2. Data for **5b**

White solid; yield: 83%; mp 94–96 °C; $^1$H NMR (600 MHz, DMSO-$d_6$) $\delta$ 7.55 (dd, $J$ = 8.4, 5.4 Hz, 2H), 7.28 (d, $J$ = 8.4 Hz, 1H), 7.18–7.15 (m, 2H), 6.76–6.75 (m, 1H), 6.56–6.54 (m, 1H), 5.09 (s, 2H), 4.56 (s, 2H); MS (EI) $m/z$: 274.17 $(M)^+$.

#### 4.4.3. Data for **5c**

White solid; yield: 69%; mp 105–106 °C; $^1$H NMR (600 MHz, DMSO-$d_6$) $\delta$ 7.52 (d, $J$ = 8.4 Hz, 1H), 7.40 (d, $J$ = 8.4 Hz, 2H), 7.27 (d, $J$ = 8.4 Hz, 2H), 6.76 (d, $J$ = 1.8 Hz, 1H), 6.54 (d, $J$ = 2.4 Hz, 1H), 5.10 (s, 2H), 4.55 (s, 2H); MS (EI) $m/z$: 290.15 $(M)^+$.

#### 4.4.4. Data for **5d**

White solid; yield: 65%; mp 118–121 °C; $^1$H NMR (600 MHz, DMSO-$d_6$) $\delta$ 7.87 (d, $J$ = 8.4 Hz, 2H), 7.70 (d, $J$ = 8.4 Hz, 2H), 7.27 (d, $J$ = 3.6 Hz, 1H), 6.74 (d, $J$ = 7.2 Hz, 1H), 6.55 (d, $J$ = 7.2 Hz, 1H), 5.09 (s, 2H), 4.64 (s, 2H); MS (EI) $m/z$: 281.19 $(M)^+$.

#### 4.4.5. Data for **5e**

White solid; yield: 84%; mp 83–84 °C; $^1$H NMR (600 MHz, $CDCl_3$) $\delta$ 7.28 (s, 1H), 7.26 (s, 1H), 7.22 (d, $J$ = 9.6 Hz, 1H), 7.19 (d, $J$ = 8.4 Hz, 1H), 6.97–6.96 (m, 1H), 6.60 (d, $J$ = 8.4 Hz, 1H), 4.52 (s, 2H), 3.68 (s, 2H); MS (EI) $m/z$: 274.24 $(M)^+$.

#### 4.4.6. Data for **5f**

White solid; yield: 78%; mp 79–81 °C; $^1$H NMR (600 MHz, $CDCl_3$) $\delta$ 7.61 (d, $J$ = 8.4 Hz, 1H), 7.41 (d, $J$ = 4.8 Hz, 1H), 7.39 (d, $J$ = 5.4 Hz, 1H), 7.26 (s, 1H), 7.21 (d, $J$ = 3.6 Hz, 2H), 6.60 (d, $J$ = 7.2 Hz, 1H), 4.47 (s, 2H), 3.71 (s, 2H); MS (EI) $m/z$: 334.18 $(M)^+$.

#### 4.4.7. Data for **5g**

White solid; yield: 76%; mp 100–102 °C; $^1$H NMR (600 MHz, DMSO-$d_6$) $\delta$ 7.63 (d, $J$ = 8.4 Hz, 2H), 7.35 (d, $J$ = 8.4 Hz, 2H), 7.28 (d, $J$ = 9.0 Hz, 1H), 6.75 (s, 1H), 6.55 (d, $J$ = 8.4 Hz, 1H), 5.09 (s, 2H), 4.60 (s, 2H); MS (EI) $m/z$: 340.21 $(M)^+$.

#### 4.4.8. Data for **5h**

White solid; yield: 71%; mp 139–141 °C; $^1$H NMR (600 MHz,

$CDCl_3$) δ 8.49 (s, 1H), 8.23 (d, $J$ = 9.0 Hz, 1H), 7.53 (d, $J$ = 8.4 Hz, 1H), 7.41 (d, $J$ = 8.4 Hz, 2H), 6.89 (d, $J$ = 9.0 Hz, 2H), 4.55 (s, 2H), 3.80 (s, 2H); MS (EI) $m/z$: 286.34 $(M)^+$.

#### 4.4.9. Data for **5i**

White solid; yield: 84%; mp 83–84 °C; $^1$H NMR (600 MHz, $CDCl_3$) δ 7.45 (s, 1H), 7.33 (s, 1H), 7.26 (s, 1H), 7.20 (d, $J$ = 7.8 Hz, 1H), 6.91 (s, 1H), 6.60 (d, $J$ = 9.0 Hz, 1H), 4.48 (s, 2H), 3.69 (s, 2H); MS (EI) $m/z$: 290.21 $(M)^+$.

#### 4.4.10. Data for **5j**

White solid; yield: 88%; mp 94–95 °C; $^1$H NMR (600 MHz, $CDCl_3$) δ 7.33 (d, $J$ = 7.8 Hz, 2H), 7.20 (d, $J$ = 8.4 Hz, 1H), 7.14 (d, $J$ = 7.8 Hz, 2H), 6.91 (s, 1H), 6.59 (d, $J$ = 6.6 Hz, 1H), 4.50 (s, 2H), 3.68 (s, 2H), 2.33 (s, 3H); MS (EI) $m/z$: 270.20 $(M)^+$.

#### 4.4.11. Data for **5k**

White solid; yield: 75%; mp 72–74 °C; $^1$H NMR (600 MHz, $CDCl_3$) δ 7.37 (s, 1H), 7.35–7.4 (m, 2H), 7.31–7.29 (m, 1H), 7.19 (d, $J$ = 9.0 Hz, 1H), 7.13 (dd, $J$ = 9.0, 2.4 Hz, 1H), 7.00 (d, $J$ = 8.4 Hz, 1H), 4.48 (s, 2H), 3.69 (s, 2H); MS (EI) $m/z$: 292.17 $(M)^+$.

### 4.5. General procedure for synthesis of the title compounds (**7**–**17**) [23]

Intermediate **5** (1.0 mmol) and 4-dimethylaminopyridine (0.1 mmol) were added to a mixture of the corresponding carboxylic acid 6 (1.3 mmol) and (EDCI, 2 mmol) in $CH_2Cl_2$ (20 mL). The reaction system was stirred at room temperature overnight and then diluted with $CH_2Cl_2$ (50 mL). The resulting mixture was consecutively washed with 10% citric acid solution and brine. Then the organic phase was dried with sodium sulphate and filtered, and concentrated under reduced pressure. The residue was purified on a silica gel column to afford the title compounds **7**–**17**.

#### 4.5.1. Data for **7a**

White solid; yield: 56%; mp 174–175 °C; $^1$H NMR (600 MHz. DMSO-$d_6$) δ 10.29 (s, 1H), 8.55 (s, 1H), 8.08 (s, 1H), 7.77 (d, $J$ = 8.4 Hz, 2H), 7.73 (d, $J$ = 7.8 Hz, 2H), 7.63 (d, $J$ = 8.4 Hz, 1H), 7.52 (d, $J$ = 8.4 Hz, 1H), 4.70 (s, 2H), 4.00 (s, 3H); $^{13}$C NMR (150 MHz, $CDCl_3$) δ 164.99, 158.78, 149.00, 141.99, 140.16, 138.61, 135.27, 134.08, 130.12, 129.90, 129.40, 125.63, 120.04, 117.29, 110.98, 109.85, 39.86 (s), 35.74 (s); HRMS (MALDI): Calcd for $C_{21}H_{14}F_6N_4O_2S$ $[M+H]^+$ 501.0820. Found: 501.0823.

#### 4.5.2. Data for **7b**

White solid; yield: 61%; mp 142–143 °C; $^1$H NMR (600 MHz, DMSO-$d_6$) δ 10.17 (s, 1H), 8.50 (s, 1H), 8.09 (s, 1H), 7.77 (d, $J$ = 7.8 Hz, 2H), 7.73 (d, $J$ = 7.8 Hz, 2H), 7.63 (d, $J$ = 9.0 Hz, 1H), 7.53 (d, $J$ = 9.0 Hz, 1H), 7.36 (t, $J$ = 54.0 Hz, 1H), 4.70 (s, 2H), 3.99 (s, 3H); $^{13}$C NMR (150 MHz, $CDCl_3$) δ 164.83, 159.49, 148.84, 143.06, 141.97, 140.18, 135.26, 134.44, 130.19, 129.87, 129.52, 125.61, 124.80, 122.99, 117.18, 116.75, 113.21, 111.67, 110.78, 110.12, 109.80, 39.60, 35.72; HRMS (MALDI): Calcd for $C_{21}H_{15}F_5N_4O_2S$ $[M+H]^+$ 483.0914. Found: 483.0914.

#### 4.5.3. Data for **8a**

White solid; yield: 47%; mp 109–111 °C; $^1$H NMR (600 MHz, DMSO-$d_6$) δ 10.29 (s, 1H), 8.54 (s, 1H), 8.07 (s, 1H), 7.63 (d, $J$ = 8.4 Hz, 1H), 7.59 (d, $J$ = 8.4 Hz, 2H), 7.57 (d, $J$ = 8.4 Hz, 1H), 7.18 (t, $J$ = 9.0 Hz, 2H), 4.62 (s, 2H), 4.00 (s, 3H); $^{13}$C NMR (150 MHz, $CDCl_3$) δ 165.34, 163.10, 161.46, 148.88, 142.21, 133.97, 131.65, 130.74, 117.13, 115.88, 115.60, 110.96, 109.75, 39.81, 35.69; HRMS (MALDI): Calcd for $C_{20}H_{14}F_4N_4O_2S$ $[M+H]^+$ 451.0852. Found: 451.0850.

#### 4.5.4. Data for **8b**

White solid; yield: 52%; mp 154–156 °C; $^1$H NMR (600 MHz, DMSO-$d_6$) δ 10.18 (s, 1H), 8.50 (s, 1H), 8.08 (d, $J$ = 2.4 Hz, 2H), 7.63 (d, $J$ = 8.4 Hz, 1H), 7.59 (dd, $J$ = 8.4, 5.4 Hz, 2H), 7.53 (dd, $J$ = 8.4, 1.8 Hz, 1H), 7.37 (d, $J$ = 7.8 Hz, 2H), 7.36 (t, $J$ = 54.6 Hz, 1H), 7.19 (t, $J$ = 9.0 Hz, 1H), 4.64 (s, 2H), 3.98 (s, 3H); $^{13}$C NMR (150 MHz, $CDCl_3$) δ 165.23, 163.09, 148.77, 142.09, 134.37, 131.66, 130.75, 116.99, 115.60, 109.73, 39.51, 35.69; HRMS (MALDI): Calcd for $C_{20}H_{15}F_3N_4O_2S$ $[M+H]^+$ 433.0946. Found: 433.0949.

#### 4.5.5. Data for **9a**

White solid; yield: 70%; mp 143–144 °C; $^1$H NMR (400 MHz, DMSO-$d_6$) δ 10.28 (s, 1H), 8.54 (s, 1H), 8.07 (d, $J$ = 1.6 Hz, 1H), 7.62 (d, $J$ = 8.8 Hz, 1H), 7.57 (s, 1H), 7.55 (s, 1H), 7.53 (dd, $J$ = 8.8, 2.0 Hz, 1H), 7.42 (s, 1H), 7.41 (d, $J$ = 1.6 Hz, 1H), 4.61 (s, 2H), 4.01 (s, 3H); $^{13}$C NMR (150 MHz, $CDCl_3$) δ 165.20, 158.93, 148.84, 141.91, 139.06, 138.93, 134.86 (s), 134.35, 133.99, 133.72, 130.37, 128.81, 121.74, 119.96, 118.17, 117.33, 116.95, 110.94, 109.71, 39.74, 35.65; HRMS (MALDI): Calcd for $C_{20}H_{14}ClF_3N_4O_2S$ $[M+H]^+$ 467.0556. Found: 467.0558.

#### 4.5.6. Data for **9b**

White solid; yield: 72%; mp 169–171 °C; $^1$H NMR (400 MHz, DMSO-$d_6$) δ 10.16 (s, 1H), 8.50 (s, 1H), 8.08 (d, $J$ = 1.6 Hz, 1H), 7.62 (d, $J$ = 8.8 Hz, 1H), 7.57 (s, 1H), 7.54 (dd, $J$ = 8.8, 2.0 Hz, 1H), 7.49 (s, 1H), 7.43 (d, $J$ = 2.0 Hz, 1H), 7.41 (d, $J$ = 2.0 Hz, 1H), 7.36 (t, $J$ = 54.0 Hz, 1H), 4.61 (s, 2H), 3.99 (s, 3H); $^{13}$C NMR (150 MHz, DMSO-$d_6$) δ 164.70, 160.33, 148.06, 145.60, 141.79, 136.20, 133.23, 132.79, 131.26, 128.88, 117.31, 116.59, 110.23, 35.13; HRMS (MALDI): Calcd for $C_{20}H_{15}ClF_2N_4O_2S$ $[M+H]^+$ 449.0651. Found: 449.0648.

#### 4.5.7. Data for **10a**

White solid; yield: 79%; mp 166–168 °C; $^1$H NMR (600 MHz, DMSO-$d_6$) δ 10.29 (s, 1H), 8.55 (s, 1H), 8.08 (s, 1H), 7.84 (d, $J$ = 7.8 Hz, 2H), 7.75 (d, $J$ = 8.4 Hz, 2H), 7.63 (d, $J$ = 8.4 Hz, 1H), 7.52 (d, $J$ = 8.4 Hz, 1H), 4.69 (s, 2H), 4.01 (s, 3H); $^{13}$C NMR (150 MHz, $CDCl_3$) δ 164.60, 158.84, 149.05, 142.00, 135.03, 134.14, 132.44, 129.83, 121.83, 120.04, 118.60, 117.33, 117.15, 111.55, 111.10, 109.99, 109.84, 39.85, 35.76; HRMS (MALDI): Calcd for $C_{21}H_{14}F_3N_5O_2S$ $[M+H]^+$ 458.0899. Found: 458.0903.

#### 4.5.8. Data for **10b**

White solid; yield: 80%; mp 223–225 °C; $^1$H NMR (600 MHz, DMSO-$d_6$) δ 10.17 (s, 1H), 8.49 (s, 1H), 8.07 (s, 1H), 7.83 (d, $J$ = 7.8 Hz, 2H), 7.74 (d, $J$ = 7.8 Hz, 2H), 7.63 (d, $J$ = 9.0 Hz, 1H), 7.51 (d, $J$ = 8.4 Hz, 1H), 7.35 (t, $J$ = 53.4 Hz, 1H), 4.64 (s, 2H), 3.98 (s, 3H); $^{13}$C NMR (150 Hz, DMSO-$d_6$) δ 164.50, 160.33, 148.08, 141.70, 136.22, 133.27, 132.83, 130.43, 117.38, 116.54, 111.00, 110.21, 110.21, 35.32; HRMS MALDI: Calcd for $C_{21}H_{15}F_2N_5O_2S$ $[M+H]^+$ 440.0993. Found: 440.0999.

#### 4.5.9. Data for **11a**

White solid; yield: 51%; mp 108–110 °C; $^1$H NMR (400 MHz, DMSO-$d_6$) δ 10.28 (s, 1H), 8.54 (s, 1H), 8.06 (d, $J$ = 2.0 Hz, 1H), 7.63 (d, $J$ = 8.8 Hz, 1H), 7.53 (dd, $J$ = 8.8, 2.0 Hz, 1H), 7.41 (s, 1H), 7.39 (d, $J$ = 1.6 Hz, 1H), 7.37 (s, 1H), 7.15–7.11 (m, 1H), 4.64 (s, 2H), 4.01 (s, 3H); $^{13}$C NMR (150 MHz, $CDCl_3$) δ 165.26, 163.54, 161.90, 158.73, 149.03, 142.17, 138.35, 135.48, 134.05, 130.24, 124.73, 121.87, 117.23, 116.10, 115.95, 115.00, 114.86, 110.96, 109.86, 39.86, 35.88; HRMS (MALDI): Calcd for $C_{20}H_{14}F_4N_4O_2S$ $[M+H]^+$ 451.0852. Found: 451.0856.

#### 4.5.10. Data for **11b**

White solid; yield: 67%; mp 128–130 °C; $^1$H NMR (600 MHz, DMSO-$d_6$) δ 10.16 (s, 1H), 8.50 (s, 1H), 8.07 (s, 1H), 7.63 (d, $J$ = 8.4 Hz, 1H), 7.54 (d, $J$ = 9.0 Hz, 1H), 7.39–7.37 (m, 3H), 7.36 (t, $J$ = 54.0 Hz,

1H), 7.13–7.11 (m, 1H), 4.63 (s, 2H), 3.99 (s, 3H); $^{13}$C NMR (150 MHz,$CDCl_3$) $\delta$ 164.86, 159.55, 150.77, 149.07, 148.90, 142.12, 135.18, 134.43, 133.19, 125.47, 118.08, 117.50, 117.28, 116.79, 113.23, 111.69, 110.86, 110.14, 109.99, 109.81, 39.55, 35.37; HRMS (MALDI): Calcd for $C_{20}H_{15}F_3N_4O_2S$ $[M+H]^+$ 433.0946. Found: 433.0939.

*4.5.11. Data for* ***12a***

White solid; yield: 74%; mp 108–110 °C; $^1$H NMR (400 MHz, DMSO-$d_6$) $\delta$ 10.27 (s, 1H), 8.53 (s, 1H), 8.05 (s, 1H), 7.75 (s, 1H), 7.61 (d, $J$ = 8.8 Hz, 1H), 7.53 (d, $J$ = 7.6 Hz, 2H), 7.48 (d, $J$ = 7.6 Hz, 1H), 7.31 (t, $J$ = 7.6 Hz, 1H), 4.61 (s, 2H), 4.00 (s, 3H); $^{13}$C NMR (150 MHz, $CDCl_3$) $\delta$ 165.08, 158.81, 148.96, 142.08, 138.82, 138.57, 138.19, 135.06, 133.98, 131.95, 130.98, 130.22, 127.68, 122.52, 121.78, 119.99, 117.19, 116.94, 110.99, 109.76, 39.78, 35.67; HRMS (MALDI): Calcd for $C_{20}H_{14}BrF_3N_4O_2S$ $[M+Na]^+$ 551.0051. Found: 551.0058.

*4.5.12. Data for* ***12b***

White solid; yield: 67%; mp 145–146 °C; $^1$H NMR (400 MHz, DMSO-$d_6$) $\delta$ 10.15 (s, 1H), 8.49 (s, 1H), 8.05 (s, 1H), 7.75 (s, 1H), 7.63 (d, $J$ = 8.4 Hz, 1H), 7.54 (d, $J$ = 6.4 Hz, 2H), 7.35 (m, 2H), 7.33 (t, $J$ = 53.6 Hz, 1H), 4.61 (s, 2H), 3.98 (s, 3H); $^{13}$C NMR (150 MHz, $CDCl_3$) $\delta$ 164.93, 159.50, 148.81, 143.07, 142.88, 142.08, 138.21, 135.00, 134.32, 131.94, 130.95, 130.20, 127.67, 122.50, 116.92, 116.63, 113.10, 111.55, 110.80, 110.00, 109.82, 39.50, 35.67; HRMS (MALDI): Calcd for $C_{20}H_{15}BrF_2N_4O_2S$ $[M+H]^+$ 493.0145. Found: 493.0152.

*4.5.13. Data for* ***13a***

White solid; yield: 65%; mp 163–165 °C; $^1$H NMR (600 MHz, DMSO-$d_6$) $\delta$ 10.29 (s, 1H), 8.55 (s, 1H), 8.08 (s, 1H), 7.68 (d, $J$ = 8.4 Hz, 2H), 7.63 (d, $J$ = 9.0 Hz, 1H), 7.53 (dd, $J$ = 8.4, 1.8 Hz, 1H), 7.36 (d, $J$ = 7.8 Hz, 2H), 4.65 (s, 2H), 4.01 (s, 3H); $^{13}$C NMR (150 MHz, $CDCl_3$) $\delta$ 165.17, 158.77, 148.84, 148.67, 142.10, 138.73, 138.49, 135.18, 134.74, 134.03, 130.51, 121.81, 121.13, 120.95, 120.03, 119.47, 117.20, 110.97, 109.96, 109.79, 39.78, 35.53; HRMS (MALDI): Calcd for $C_{21}H_{14}F_6N_4O_2S$ $[M+H]^+$ 517.0769. Found: 517.0774.

*4.5.14. Data for* ***13b***

White solid; yield: 45%; mp 111–113 °C; $^1$H NMR (600 MHz, DMSO-$d_6$) $\delta$ 10.18 (s, 1H), 8.51 (s, 1H), 8.09 (s, 1H), 7.68 (d, $J$ = 8.4 Hz, 2H), 7.64 (d, $J$ = 9.0 Hz, 1H), 7.54 (d, $J$ = 9.0 Hz, 1H), 7.37 (d, $J$ = 7.8 Hz, 2H), 7.36 (t, $J$ = 54.0 Hz, 1H), 4.64 (s, 2H), 3.98 (s, 3H); $^{13}$C NMR (150 MHz, DMSO-$d_6$) $\delta$ 165.07, 159.51, 148.75, 143.03, 141.99, 135.15, 134.72, 134.41, 130.51, 121.12, 119.46, 117.14, 116.74, 113.17, 111.62, 110.74, 110.08, 109.76, 39.56, 35.52; HRMS (MALDI): Calcd for $C_{21}H_{15}F_5N_4O_2S$ $[M+H]^+$ 499.0863. Found: 499.0857.

*4.5.15. Data for* ***14a***

White solid; yield: 62%; mp 166–168 °C; $^1$H NMR (400 MHz, DMSO-$d_6$) $\delta$ 10.27 (s, 1H), 8.54 (s, 1H), 8.05 (d, $J$ = 1.6 Hz, 1H), 7.62 (d, $J$ = 8.8 Hz, 1H), 7.53 (d, $J$ = 1.6 Hz, 1H), 7.44 (d, $J$ = 8.4 Hz, 2H), 6.91 (d, $J$ = 8.4 Hz, 2H), 4.57 (s, 2H), 4.00 (s, 3H), 3.73 (s, 3H); $^{13}$C NMR (150 MHz, $CDCl_3$) $\delta$ 165.71, 159.20, 158.87, 148.84, 142.17, 138.73, 134.82, 133.90, 130.26, 127.48, 121.77, 119.98, 117.12, 114.05, 110.94, 109.65, 55.20, 39.70, 36.08; HRMS (MALDI): Calcd for $C_{21}H_{17}F_3N_4O_3S$ $[M+Na]^+$ 485.0871. Found: 485.0868.

*4.5.16. Data for* ***14b***

White solid; yield: 64%; mp 163–165 °C; $^1$H NMR (400 MHz, DMSO-$d_6$) $\delta$ 10.16 (s, 1H), 8.50 (s, 1H), 8.07 (s, 1H), 7.62 (d, $J$ = 8.8 Hz, 1H), 7.52 (d, $J$ = 8.8 Hz, 1H), 7.45 (d, $J$ = 8.4 Hz, 2H), 7.35 (t, $J$ = 56.0 Hz, 1H), 6.90 (d, $J$ = 8.4 Hz, 2H), 4.57 (s, 2H), 3.98 (s, 3H), 3.73 (s, 3H); $^{13}$C NMR (150 MHz, $CDCl_3$) $\delta$ 165.68, 159.57, 159.25, 148.80, 142.30, 134.99, 134.33, 130.33, 127.63, 117.06, 114.12, 111.60, 110.81, 109.73, 55.27, 39.55, 36.16; HRMS (MALDI): Calcd for $C_{21}H_{18}F_2N_4O_3S$ $[M+H]^+$ 445.1146. Found: 445.1145.

*4.5.17. Data for* ***15a***

White solid; yield: 62%; mp 95–97 °C; $^1$H NMR (600 MHz, $CDCl_3$) $\delta$ 10.27 (s, 1H), 8.54 (s, 1H), 8.06 (s, 1H), 7.94 (s, 1H), 7.91 (s 1H), 7.53 (s, 1H), 7.47 (s, 1H), 7.38 (s, 1H), 7.36 (d, $J$ = 4.2 Hz, 1H), 4.51 (s, 2H), 3.99 (s, 3H); $^{13}$C NMR (151 MHz, $CD_3OD$-$d_6$) $\delta$ 167.07, 161.80, 150.39, 143.46, 142.39, 140.71, 137.04, 135.81, 135.31, 131.66, 130.57, 129.41, 128.99, 119.15, 118.33, 112.19, 111.26, 40.41 (s), 36.79 (s); HRMS (MALDI): Calcd for $C_{20}H_{14}ClF_3N_4O_2S$ $[M+H]^+$ 467.0556. Found: 467.0562.

*4.5.18. Data for* ***15b***

White solid; yield: 66%; mp 151–152 °C; $^1$H NMR (600 MHz, DMSO-$d_6$) $\delta$ 10.25 (s, 1H), 8.25 (s, 1H), 8.06 (s, 1H), 7.97 (s, 1H), 7.47 (s, 1H), 7.43 (d, $J$ = 8.4 Hz, 1H), 7.39–7.35 (m, 2H), 7.27 (s, 1H), 6.92 (t, $J$ = 54.6 Hz, 1H), 4.52 (s, 2H), 3.96 (s, 3H); $^{13}$C NMR (150 MHz, $CDCl_3$) $\delta$ 165.00, 159.37, 148.82, 142.84, 142.04, 137.94, 135.35, 134.42, 129.94, 129.09, 128.07, 127.22, 117.10, 116.84, 113.29, 111.71, 110.73, 109.97, 39.61, 35.78; HRMS (MALDI): Calcd for $C_{20}H_{15}ClF_2N_4O_2S$ $[M+H]^+$ 449.0651. Found: 449.0648.

*4.5.19. Data for* ***16a***

White solid; yield: 76%; mp 139–140 °C; $^1$H NMR (600 MHz, DMSO-$d_6$) $\delta$ 10.29 (s, 1H), 8.55 (s, 1H), 8.06 (s, 1H), 7.63 (d, $J$ = 9.0 Hz, 1H), 7.54 (d, $J$ = 9.0 Hz, 1H), 7.40 (d, $J$ = 7.8 Hz, 2H), 7.16 (d, $J$ = 7.8 Hz, 2H), 4.58 (s, 2H), 4.01 (s, 3H), 2.27 (s, 3H); $^{13}$C NMR (150 MHz, $CDCl_3$) $\delta$ 165.64, 159.10, 148.69, 141.82, 139.75, 139.32, 137.71, 134.39, 133.92, 132.32, 129.35, 128.86, 121.69, 119.91, 117.41, 116.77, 110.94, 109.54, 39.59 36.21, 21.03; HRMS (MALDI): Calcd for $C_{21}H_{17}F_3N_4O_2S$ $[M+H]^+$ 447.1103. Found: 447.1095.

*4.5.20. Data for* ***16b***

White solid; yield: 54%; mp 117–119 °C; $^1$H NMR (600 MHz, DMSO-$d_6$) $\delta$ 10.17 (s, 1H), 8.50 (s, 1H), 8.06 (s, 1H), 7.63 (s, 1H), 7.62 (d, $J$ = 8.4 Hz, 1H), 7.53 (d, $J$ = 8.4 Hz, 1H), 7.40 (d, $J$ = 7.8 Hz, 2H), 7.36 (t, $J$ = 54.6 Hz, 1H), 4.58 (s, 2H), 3.98 (s, 3H), 2.27 (s, 3H); $^{13}$C NMR (100 MHz, DMSO-$d_6$) $\delta$ 164.47, 159.89, 147.58, 141.44, 136.96, 133.34, 132.85, 129.08, 129.00, 116.87, 116.14, 109.79, 35.40, 20.63; HRMS (MALDI): Calcd for $C_{21}H_{18}F_2N_4O_2S$ $[M+H]^+$ 429.1197. Found: 429.1204.

*4.5.21. Data for* ***17a***

White solid; yield: 59%; mp 121–123 °C; $^1$H NMR (400 MHz, DMSO-$d_6$) $\delta$ 10.28 (s, 1H), 8.55 (s, 1H), 8.07 (s, 1H), 7.64 (s, 1H), 7.61 (d, $J$ = 5.2 Hz, 1H), 7.53 (d, $J$ = 8.8 Hz, 1H), 7.42 (t, $J$ = 6.8 Hz, 2H), 4.61 (s, 2H), 4.01 (s, 3H). $^{13}$C NMR (150 MHz, $CDCl_3$) $\delta$ 164.99, 158.69, 150.80, 149.02, 142.08, 135.45, 134.06, 133.12, 125.21, 121.84, 120.05, 118.07, 117.49, 117.31, 110.97, 109.86, 39.86, 35.37; HRMS (MALDI): Calcd for $C_{20}H_{13}F_5N_4O_2S$ $[M+H]^+$ 469.0758. Found: 469.0760.

*4.5.22. Data for* ***17b***

White solid; yield: 49%; mp 142–144 °C; $^1$H NMR (400 MHz, DMSO-$d_6$) $\delta$ 10.17 (s, 1H), 8.51 (s, 1H), 8.09 (d, $J$ = 1.6 Hz, 1H), 7.65 (d, $J$ = 5.6 Hz, 1H), 7.62–7.60 (m, 1H), 7.55 (dd, $J$ = 8.8, 2.0 Hz, 1H), 7.43–7.40 (m, 2H), 7.37 (t, $J$ = 54 Hz, 1H), 4.62 (s, 2H), 3.99 (s, 3H); $^{13}$C NMR (150 MHz, $CDCl_3$) $\delta$ 164.80, 159.49, 150.71, 149.02, 148.85, 142.07, 135.13, 134.37, 133.14, 125.41, 118.03, 117.45, 117.23, 116.74 (s), 113.18, 111.63, 110.81, 110.09, 109.93, 109.75, 39.50, 35.32; HRMS (MALDI): Calcd for $C_{20}H_{14}F_4N_4O_2S$ $[M+H]^+$ 451.0852. Found: 451.0850.

### *4.6. Enzymatic kinetics [24–26]*

The preparation of succinate-cytochrome *c* reductase (SCR, mixture of respiratory SQR and complex III) from porcine heart was essentially as reported. The activity of SCR was measured by

monitoring the increase of cytochrome *c* at 550 nm, by using the extinction coefficient of 18.5 $mM^{-1}$ $cm^{-1}$. The succinate–ubiquinone reductase (SQR) activity was measured by monitoring the decrease of 2,6-dichlorophenolindophenol (DCIP) at 600 nm, by using the extinction coefficient of 21 $mM^{-1}$ $cm^{-1}$. The reaction mixture may be scaled down to 1.8 mL with final concentrations of PBS (pH 7.4), 100 mM; EDTA, 0.3 mM; succinate, 20 mM; oxidized cytochrome *c*, 60 μM (or DCIP, 53 μM); and appropriate amounts of enzyme to start the reaction. The ubiquinol–cytochrome *c* reductase (complex III) activity in catalysing the oxidation of $DBH_2$ by cytochrome *c* was assayed in 100 mM PBS (pH 7.4), 0.3 mM EDTA, 750 μM lauryl maltoside (*n*-dodecyl-β-D-maltoside), 100 μM $DBH_2$, 100 μM oxidized cytochrome *c*, and an appropriate amount of SCR. The preparation of $DBH_2$ from DB was carried out according to the procedure described in previous publications [11], and the concentration of $DBH_2$ was determined by measuring the absorbance difference between 288 and 320 nm using an extinction coefficient of 4.14 $nM^{-1}$ $cm^{-1}$ for the calculation [27,28].

For the steady state studies, the reaction was carried out in the absence or presence of various concentrations of the inhibitor. To obtain the $K_i$ and $IC_{50}$ values, all reactions were initiated by the addition of enzyme and monitored continuously by following the absorbance change at certain wavelengths on a Perkin–Elmer Lambda 45 spectrophotometer equipped with a magnetic stirrer at 23 °C.

### 4.7. Data analysis [29]

First, according to the measured substances extinction coefficient, the change of absorbance was converts to product variation, then making linear fitting of time, the slope is the enzymatic reaction velocity. Compared with the control sample, the inhibition rates of inhibitors were calculated. The concentrations at 50% inhibition (absolute $IC_{50}$ values) for experiments with SCR were obtained from a nonlinear regression of the activity data according to a four parameter logistic model. The absolute $IC_{50}$ was calculated according to Eq. (1)

$$y = \min + \frac{\max - \min}{1 + 10^{x - \log IC_{50}}} \quad (1)$$

Where y is the percentage of maximal rate, max and min are the y values at which the curve levels off, x is the logarithm of inhibitor concentration, and $IC_{50}$ is the concentration of inhibitor that caused 50% of the total inhibition.

The inhibition type was determined by Lineweaver–Burk plots, and computer fitted to the appropriate equations like Eqs. (2) and (3). Sigma Plot software 9.0 was used to determine all kinetic constants.

$$v = \frac{V_{max}[S]}{\left(1 + \frac{[I]}{K_i}\right)K_m + [S]} \quad (2)$$

$$v = \frac{V_{max}[S]}{\left(1 + \frac{[I]}{K_i}\right)(K_m + [S])} \quad (3)$$

### 4.8. Molecular docking

The crystal structure of 1ZOY from porcine was selected as receptor. As we know, SQR consisted of four subunits (A, B, C, and D) and the binding site (Q-site) of ligand was formed by the subunits B, C, and D. So, chain A was deleted in the following molecular docking and binding free energy calculations.

The docking procedure was similar with our previous study [11]. The AutoDock 4.2 program [30] was applied to dock these inhibitors into the Q-site. Gasteiger charges were used for these inhibitors. In the docking process, a conformational search was performed for ligand, using the Solis and Wets local search method. The Lamarkian genetic algorithm (LGA) [31,32] was applied for the conformational search of the binding complex of ligand with porcine 1ZOY. Among a series of docking parameters, the grid size was set as 40 × 32 × 40, and the grid space used was set to the default value of 0.375 Å. The interaction energy, which resulted from probing the porcine SQR with ligand, was assessed using the standard AutoDock scoring function. Among a set of 256 candidates of the docked complex structures, the best one was first selected based on the interaction energy and the binding mode of commercial carboxamide fungicides obtained from our previous study [11].

All the complex structures derived from molecular docking were used as starting structures for further energy minimizations, using the Sander module of the Amber8 [33] program before the final binding structures were achieved. Firstly, the ligand was minimized with the protein fixed. Secondly, the backbone atoms of the protein were fixed, and other atoms were relaxed. The final minimization was performed with both the ligand and the protein relaxed. In each step, the energy minimization was executed by using the steepest descent method for the first 1000 cycles, and the conjugated gradient method for the subsequent 2000 cycles with a convergence criterion of 0.1 kcal $mol^{-1}$ $Å^{-1}$. Then, an additional 20 ps MD simulation was performed. For temperature regulation, the Langevin thermostat was used to maintain a temperature of 300 K. The atomic coordinates were saved per ps. Subsequently, the last snapshot of the MD simulation was minimized to a convergence criterion of 0.1 kcal $mol^{-1}$ $Å^{-1}$. Then, the ΔH calculation was performed on the minimized complex. The bcc charges were used as the atomic charges for these inhibitors. The energy minimization process was the same as previously described [11].

### 4.9. Binding energy calculation

On the basis of the modelled complex structure of porcine SQR bound with inhibitors, the binding free energy for each of the minimized complexes was estimated using the molecular mechanics-Possion-Boltzmann surface area (MM-PBSA) method [34]. In this method, the binding free energy of the protein-ligand complex ($\Delta G_{bind}$) is obtained from the difference between the free energies of the protein-ligand complex ($\Delta G_{cpx}$) and the unbound receptor ($\Delta G_{rec}$) and the free ligand ($\Delta G_{lig}$) as follows: [35].

$$\Delta G_{bind} = \Delta G_{cpx} - \Delta G_{rec} - \Delta G_{lig} \quad (4)$$

Binding free energy ($\Delta G_{bind}$) can be evaluated as sum of the changes in molecular mechanical (MM) gas-phase binding energy ($\Delta E_{MM}$), solvation free energy ($\Delta G_{sol}$), and entropic contribution ($-T\Delta S$). The $\Delta E_{MM}$ was evaluated as a sum of electrostatic energy ($\Delta E_{ele}$) and van der Waals interaction energy ($\Delta E_{vdw}$).

$$\Delta G_{bind} = \Delta E_{MM} + \Delta G_{sol} - T\Delta S \quad (5)$$

$$\Delta E_{MM} = \Delta E_{ele} + \Delta E_{vdw} \quad (6)$$

The solvation free energy $\Delta G_{sol}$ was composed of two parts:

$$\Delta G_{sol} = \Delta G_{PB} + \Delta G_{np} \quad (7)$$

$$\Delta G_{np} = \gamma SASA + \beta \quad (8)$$

The electrostatic contribution to the solvation free energy ($\Delta G_{PB}$) was evaluated using Poisson-Boltzmann (PB) methods [36,37]. The nonpolar solvation energy, $\Delta G_{np}$, can be estimated by an empirical relation of $\Delta G_{np} = \gamma SASA + \beta$, where SASA is defined as the solvent-accessible surface area, and the solvation parameters $\gamma$ and $\beta$ were set to 0.00542 kcal mol$^{-1}$ Å$^{-2}$ and 0.92 kcal mol$^{-1}$ respectively. The dielectric constant for the molecule and surrounding solvent were set to 1 and 80, respectively, while the probe radius of the solvent was set to 1.4 Å.

The entropy contribution to the binding free energy can be divided into two parts: the solvation free entropy ($\Delta S_{solv}$) and the conformational free entropy ($\Delta S_{conf}$).

$$\Delta S_{sol} = \Delta S_{solv} + \Delta S_{conf} \quad (9)$$

The solvation free entropy is gained by the tendency of water molecules to minimize their contacts with hydrophobic groups in protein. The conformational free entropy is related to the change of the number of rotatable bonds during the binding process. The detailed computational procedure used to evaluate the entropy contribution ($-T\Delta S$) to the binding free energy was the same as previously described [38].

## Acknowledgements

The research was supported in part by the National Key Technologies R&D Program (2011BAE06B05) and the National Natural Science Foundation of China (No. 21332004 and 21272092).

## Appendix A. Supplementary data

Supplementary data related to this article can be found at http://dx.doi.org/10.1016/j.ejmech.2015.03.060.

## References

[1] G. Cecchini, Function and structure of complex II of the respiratory chain, Annu. Rev. Biochem. 72 (2003) 77–109.
[2] E. Maklashina, G. Cecchini, The quinone-binding and catalytic site of complex II, Biochim. Biophys. Acta 1797 (2010) 1877–1882.
[3] F. Sun, X. Huo, Y. Zhai, A. Wang, J. Xu, D. Su, M. Bartlam, Z. Rao, Crystal structure of mitochondrial respiratory membrane protein complex II, Cell 121 (2005) 1043–1057.
[4] V. Yankovskaya, R. Horsefield, S. Tornroth, C. Luna-Chavez, H. Miyoshi, C. Leger, B. Byrne, G. Cecchini, S. Iwata, Architecture of succinate dehydrogenase and reactive oxygen species generation, Science 299 (2003) 700–704.
[5] C. Hägerhäll, Succinate: quinone oxidoreductases: variations on a conserved theme, Biochim. Biophys. Acta 1320 (1997) 107–141.
[6] N. Ishii, M. Fujii, P.S. Hartman, M. Tsuda, K. Yasuda, N. Senoo-Matsuda, S. Yanase, D. Ayusawa, K. Suzuki, A mutation in succinate dehydrogenase cytochrome *b* causes oxidative stress and ageing in nematodes, Nature 394 (1998) 694–697.
[7] N. Senoo-Matsuda, K. Yasuda, M. Tsuda, T. Ohkubo, S. Yoshimura, H. Nakazawa, P.S. Hartman, N. Ishii, A defect in the cytochrome b large subunit in complex II causes both superoxide anion overproduction and abnormal energy metabolism in Caenorhabditis elegans, J. Biol. Chem. 276 (2001) 41553–41558.
[8] P. Rustin, A. Rötig, Inborn errors of complex II—unusual human mitochondrial diseases, Biochim. Biophys. Acta 1553 (2002) 117–122.
[9] L. Carvalho, R.L.O. Juan, L.M. Carmen, C. Santiago, R. Luis, G. Francisco, The 8-aminoquinoline analogue sitamaquine causes oxidative stress in Leishmania donovani promastigotes by targeting succinate dehydrogenase, Antimicrob. Agents Chemother. 55 (2011) 4204–4210.
[10] Mode of Action of Fungicides. FRAC Classification on Mode of Action, Crop Life, 2014. http://www.frac.info.
[11] X.L. Zhu, L. Xiong, H. Li, X.Y. Song, J.J. Liu, G.F. Yang, Computational and experimental insight into the molecular mechanism of carboxamide inhibitors of succinate-ubquinone oxidoreductase, ChemMedChem 9 (2014) 1512–1521.
[12] Y.H. Ye, L. Ma, Z.C. Dai, Y. Xiao, Y.Y. Zhang, D.D. Li, J.X. Wang, H.L. Zhu, Synthesis and antifungal activity of nicotinamide derivatives as succinate dehydrogenase inhibitors, J. Agric. Food Chem. 62 (2014) 4063–4071.
[13] M. Hiroko, S. Kazuro, U. Hideaki, Y. Yuichi, M. Rokuro, T. Hiroshi, M. Hideto, O. Arihiro, K. Kiyoshi, O. Satoshi, Atpenins, potent and specific inhibitors of mitochondrial complex II (succinate-ubiquinone oxidoreductase), Proc. Natl. Acad. Sci. U. S. A. 100 (2003) 473–477.
[14] H. Walter, Bioactive Heterocyclic Compound Classes: Agrochemicals, Wiley-VCH Verlag GmbH & Co. KGaA, 2012, pp. 177–193.
[15] L.Q. Sun, J. Chen, M. Bruce, J.A. Deskus, J.R. Epperson, K. Takaki, G. Johnson, L. Iben, C.D. Mahle, E. Ryan, C. Xu, Synthesis and structure-activity relationship of novel benzoxazole derivatives as melatonin receptor agonists, Bioorg. Med. Chem. Lett. 14 (2004) 3799–3802.
[16] D. Seenaiah, P.R. Reddy, G.M. Reddy, A. Padmaja, V. Padmavathi, N. Siva krishna, Synthesis, antimicrobial and cytotoxic activities of pyrimidinyl benzoxazole, benzothiazole and benzimidazole, Eur. J. Med. Chem. 77 (2014) 1–7.
[17] A. Sun, A. Prussia, W. Zhan, E.E. Murray, J. Doyle, L.T. Cheng, J.J. Yoon, E.V. Radchenko, V.A. Palyulin, R.W. Compans, D.C. Liotta, R.K. Plemper, J.P. Snyder, Nonpeptide inhibitors of measles virus entry, J. Med. Chem. 49 (2006) 5080–5092.
[18] A. Jeanguenat, G. Hall-Roger, O. Loiseleur, S. Trah, P. Durieux, A. Edmunds, A. Stoller. Novel Insecticides. WO2007/020050 (USA 2007).
[19] J. Rheinheimer, H. Rieck, P.Y. Coqueron, Modern Crop Protection Compounds, Wiley-VCH Verlag GmbH & Co. KGaA, 2012, pp. 627–633.
[20] D.S.B. Ongarora, J. Gut, P.J. Rosenthal, C.M. Masimirembwa, K. Chibale, Benzoheterocyclic amodiaquine analogues with potent antiplasmodial activity: synthesis and pharmacological evaluation, Bioorg. Med. Chem. Lett. 22 (2012) 5046–5050.
[21] Z. Yang, S.G. Yang, Y.P. Luo, Y. Tan, G.F. Hao, Q.Y. Wu, Z. Xi, G.F. Yang, Design and synthesis of 1-(benzothiazol-5-yl)-1H-1,2,4-triazol-5-ones as protoporphyrinogen oxidase inhibitors, Bioorg. Med. Chem. 21 (2013) 3245–3255.
[22] L.L. Jiang, Y. Tan, X.L. Zhu, Z.F. Wang, Y. Zuo, Q. Chen, Z. Xi, G.F. Yang, Design, synthesis, and 3D-QSAR analysis of novel 1,3,4-oxadiazol-2(3H)-ones as protoporphyrinogen oxidase inhibitors, J. Agric. Food Chem. 58 (2009) 2643–2651.
[23] R.P. Tangallapally, R. Yendapally, R.E. Lee, K. Hevener, V.C. Jones, A.J.M. Lenaerts, M.R. McNeil, Y. Wang, S. Franzblau, R.E. Lee, Synthesis and evaluation of nitrofuranylamides as novel antituberculosis agents, J. Med. Chem. 47 (2004) 5276–5283.
[24] G.F. Hao, F. Wang, H. Li, X.L. Zhu, W.C. Yang, L.S. Huang, J.W. Wu, E.A. Berry, G.F. Yang, Computational discovery of picomolar $Q_o$ site inhibitors of cytochrome $bc_1$ complex, J. Am. Chem. Soc. 134 (2012) 11168–11176.
[25] P.L. Zhao, L. Wang, X.L. Zhu, X. Huang, C.G. Zhan, J.W. Wu, G.F. Yang, Subnanomolar inhibitor of cytochrome $bc_1$ complex designed by optimizing interaction with conformationally flexible residues, J. Am. Chem. Soc. 132 (2010) 185–194.
[26] T.E. King, Preparations of succinate-cytochrome *c* reductase and the cytochrome $bc_1$ particle, and reconstitution of succinate-cytochrome c reductase, Methods Enzymol. 10 (1967) 216–225.
[27] N. Fisher, I. Bourges, P. Hill, G. Brasseur, B. Meunier, Disruption of the interaction between the Rieske iron-sulfur protein and cytochrome *b* in the yeast $bc_1$ complex owing to a human disease-associated mutation within cytochrome *b*, Eur. J. Biochem. 271 (2004) 1292–1298.
[28] N. Fisher, A.C. Brown, G. Sexton, A. Cook, J. Windass, B. Meunier, Modeling the $Q_o$ site of crop pathogens in *Saccharomyces cerevisiae* cytochrome *b*, Eur. J. Biochem. 271 (2004) 2264–2271.
[29] F. Wang, H. Li, L. Wang, W.C. Yang, J.W. Wu, G.F. Yang, Design, syntheses, and kinetic evaluation of 3-(phenylamino)oxazolidine-2,4-diones as potent cytochrome $bc_1$ complex inhibitors, Bioorg. Med. Chem. 19 (2011) 4608–4615.
[30] G.M. Morris, R. Huey, W. Lindstrom, M.F. Sanner, R.K. Belew, D.S. Goodsell, A.J. Olson, AutoDock4 and AutoDockTools4: automated docking with selective receptor flexibility, J. Comput. Chem. 30 (2009) 2785–2791.
[31] G.M. Morris, D.S. Goodsell, R.S. Halliday, R. Huey, W.E. Hart, R.K. Belew, A.J. Olson, Automated docking using a Lamarckian genetic algorithm and and empirical binding free energy function, J. Comput. Chem. 19 (1998) 1639–1662.
[32] D. Sitkoff, K.A. Sharp, B. Honig, Accurate calculation of hydration free energies using macroscopic solvent models, J. Phys. Chem. 98 (1994) 1978–1988.
[33] D.A. Case, et al., AMBER 8, University of California, San Francisco, CA, 2004.
[34] P.A. Kollman, I. Massova, C. Reyes, B. Kuhn, S. Huo, L. Chong, M. Lee, Y. Duan, W. Wang, O. Donini, P. Cieplak, J. Srnivasan, D.A. Case, T.E. Cheatham, Calculating structures and free energies of complex molecules: combining molecular mechanics and continuum models, Acc. Chem. Res. 33 (2000) 889–897.
[35] M.L. Connolly, Analytical molecular surface calculation, J. Appl. Cryst. 16 (1983) 548–558.
[36] B. Jayaram, K.A. Sharp, B. Honig, The electrostatic potential of B-DNA, Biopolymers 28 (1989) 975–993.
[37] M.F. Sanner, A.J. Olson, J.C. Spehner, Reduced surface: an efficient way to compute molecular surfaces, Biopolymers 38 (1996) 305–320.
[38] Y.M. Pan, D.Q. Gao, C.G. Zhan, Modeling the catalysis of anti-cocaine catalytic antibody: competing reaction pathways and free energy barriers, J. Am. Chem. Soc. 130 (2008) 5140–5149.